Accepted Manuscript

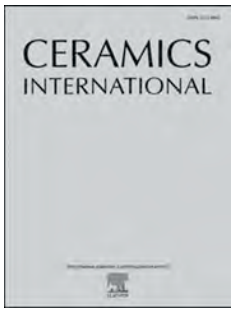

Investigation on glass-forming ability,Flexural strength and microwave dielectric properties of Al_2O_3-doped LMZBS glasses

Tianying Qin, Chaowei Zhong, Hongcheng Yang, Yang Qin, Shuren Zhang

PII: S0272-8842(19)30469-9

DOI: https://doi.org/10.1016/j.ceramint.2019.02.168

Reference: CERI 20891

To appear in: *Ceramics International*

Received Date: 11 December 2018

Revised Date: 18 February 2019

Accepted Date: 24 February 2019

Please cite this article as: T. Qin, C. Zhong, H. Yang, Y. Qin, S. Zhang, Investigation on glass-forming ability,Flexural strength and microwave dielectric properties of Al_2O_3-doped LMZBS glasses, *Ceramics International* (2019), doi: https://doi.org/10.1016/j.ceramint.2019.02.168.

Investigation on Glass-forming ability、Flexural strength and Microwave dielectric properties of Al_2O_3-doped LMZBS glasses

Tianying Qin[1, 2], Chaowei Zhong[1, 2], Hongcheng Yang[1, 2], Yang Qin[1, 2], and Shuren Zhang, [1, 2]

1. School of Electronic Science and Engineering, University of Electronic Science and Technology of China, Chengdu 610054, People's Republic of China.

2. Key Laboratory of Multi-Spectral Absorbing Materials and Structures of Ministry of Education, University of Electronic Science and Technology of China.

ABSTRACT: In this work, a new high flexural strength microwave dielectric material for LTCC applications, (1-x) Li_2O-MgO-ZnO-B_2O_3-SiO_2-xAl_2O_3 (x=1~10wt. %) (LMZBSA) glass-ceramics, was prepared by conventional solid-state reaction method. The effects of Al_2O_3-doped Li2O-MgO-ZnO-B_2O_3-SiO2 (LMZBS) glass on its glass-forming ability (GFA) and activation energy were investigated by Dietzel, Saad-Paulin methods and Kissinger model, respectively. Comparing the undoped sample with the 10wt. % of Al_2O_3-doped LMZBS glass the parameters of ΔT and S which characterize the GFA increase by 35% and twice, respectively. Meanwhile, the addition of Al_2O_3 will reduce the activation energy, making initial crystallization easier. And then the impact of Al_2O_3 on the phase composition, flexural strength and microwave dielectric properties of LMZBSA glass-ceramics was studied systematically. It shows that the content of Al_2O_3 has a great influence on the flexural strength of LMZBSA glass-ceramics, and different composition is responsible for its microwave dielectric properties. LMZBSA glass-ceramics with 5wt. % Al_2O_3 sintered 2h at 900℃ showed the highest relative density (96.41%) and flexural strength (σ =190MPa), optimum microwave dielectric properties (ε_r=6.8, $Q\times f$=12500GHz, τ_f=-45ppm/℃).

KEYWORDS: Glass-forming ability, LMZBSA glass-ceramic, Flexural strength,

Microwave dielectric properties.

1. INTRODUCTION

To meet the requirement of integration， modularization and miniaturization of electronic components, low temperature co-fired ceramic (LTCC) materials are widely used in passive devices (capacitors, inductors, etc.) working at microwave frequencies. For LTCC application, materials with desired dielectric properties should be sintered at a low temperature (below 950℃), and can be co-fired with Ag, Cu or other high conductivity metals [1-4].

Glass is often used as sintering aids to reduce the sintering temperature of the ceramic-based materials by liquid-phase sintering. Among the various glasses, Li_2O-MgO-ZnO-B_2O_3-SiO_2 (LMZBS) glass has been proven to be an appropriate addition for lowering the sintering temperature of $MgAl_2O_4$, Li $(Zn_{0.95}Co_{0.05})_{1.5}SiO_4$, $SrCuSi_4O_{10}$, Li_2MgSiO_4, $Mg_3B_2O_6$, $Li_3Mg_{1.8}Ca_{0.2}NbO_6$ ceramics [5-10]. And Xie et al. had systematically reported the microstructure of LMZBS glass-ceramics could be improved by changing the amount of MgO, and the sample with a flexural strength of 160 MPa can be obtained when sintered at 920 °C[11].

It has been proposed that the addition of Al_2O_3 to the MgO-B_2O_3-SiO_2 glass system can improve their GFA and sintering densification[12]. The purpose of this paper is investigating the effect of different amounts of Al_2O_3 on the sintered crystallization behavior and microwave dielectric properties of the LMZBSA glass-ceramics. In order to emphasize the influence of Al_2O_3 on crystallization tendency of LMZBS glass, their GFA were also discussed.

2. Experimental procedures

The LMZBS glass doped with Al_2O_3 were synthesized from highly purified powders provided by CHRON CHEMISTRY: Li_2CO_3, MgO, ZnO, H_3BO_3, SiO_2, and Al_2O_3.The glass compositions were weighed based on stoichiometric ratio of (100-x) (Li_2O-MgO-ZnO-B_2O_3-SiO_2) +xAl_2O_3, (x=0~10wt. %.), which was melted at 1350℃ in a platinum crucible, quenched and powdered.

DSC curve (heating rate is 10℃/min) was obtained from Thermomechanical Analysis (TMA) (Model DIL 420C, Netzsch, Germany) to explore the GFA of

LMZBS glass. Meanwhile, the activation energy (E_a) was investigated, a few heating rates were adopted during the DSC equipment (5.0, 7.5, 10.0, and15.0K/min).

The fine powder sample was mixed with acrylic emulsion and granulated, and then molded at a pressure of 20 MPa to get a green cylinder（Φ=15mm×7.5mm） and a strip（Φ=50mm×4mm×4mm）to measure the dielectric properties and strength. The final dense glass-ceramics sample was synthesized in air atmosphere at 900℃ for 2h and naturally cooled.

A range of tests for LMZBSA glass-ceramics were listed as follows: the relative density was obtained by calculated. The crystal phase information was verified by X-ray diffraction (XRD, PANalytical PW3040/60, Netherlands) with scanning angles 2θ of 10°to 120°using Cu K_α radiation. Crystallographic information obtained through refining XRD data using the GSAS-EXPGUI program. The morphology of the as-fired surface was observed with a scanning electron microscope (SEM, FEI Inspect F, and the UK). Microwave dielectric properties were measured in the TE011 mode by a Hakki-Coleman dielectric resonator method using a network analyzer (HP83752A, USA). The flexural strength was determined by three-point bending method with an electromechanical Universal testing machine (MTS CMT6104, China). The τ_f value was estimated from the following formula (1):

$$\tau_f = \frac{f_{85} - f_{25}}{f_{25} \times 60} \times 10^6 \, (ppm \cdot ℃^{-1}) \quad (1)$$

Where f_{25} and f_{85} are the resonant frequencies measured at 25 and 85℃, respectively.

3. RESULTS AND DISCUSSION

3.1 Exploration of glass forming ability

The DSC curve of the LMZBS glass with 10wt. % Al_2O_3 was obtained at the heating rate of 10K/min, as shown in **F**ig.1. The characteristic temperatures T_g=778℃ (glass transition temperature), T_x=907℃ (onset crystallization temperature), and T_p=966℃ (crystallization peak temperature) for this glass specimen were observed. Table1 lists the relevant temperatures for different compositions. T_x and T_p increased approximately 3 and 4%, respectively, after adding Al_2O_3.

The GFA of the selected compositions can be quantitatively determined by Dietzel and Saad-Paulin methods, such as equation (2) and (3) [13, 14]:

$$\text{Dietzel:} \quad \Delta T = T_p - T_g \tag{2}$$

$$\text{Saad-Paulin:} \quad S = (T_p - T_x)(T_x - T_g)/T_g \tag{3}$$

Where the ΔT and S are parameter to characterize the GFA, and the glass with larger ΔT and S values will show a greater tendency for GFA. The values are also summarized in Table 1. For the 10wt. % of Al_2O_3-doped LMZBS glass ΔT increase by 35% and S increase twice comparing with the undoped sample.

The activation energy (E_a) of sintering crystallization of these glasses was investigated by analyzing DSC curves of different sintering rates of 5, 7.5, 10, 15K/min. Fig.2 (a) shows the crystallization peak displacements at different heating rates for the LMZBS with 5wt. % of Al_2O_3. As shown in Fig.2 (a), the glass crystallization behaviors are switch to a higher temperature with the sintering rate increase. This phenomenon indicates that the crystallization processes are thermally activated[13]. The Kissinger model is the most commonly employed kinetic model for any thermally activated solid state reaction, which can be used to depict the crystallization behaviors. The activation energy (E_a) can be evaluated using the Kissingger model[15]:

$$In(\frac{T_p^2}{\phi}) = \frac{E_a}{RT_P} + C \tag{4}$$

Where C is constant, R is the gas constant. Following to equation (4), a linear fitting of the plot of $In(T_p^2/\phi)$ vs $1000/T_p$ can be adopted to calculate the E_a, and the diagrams are shown in Fig.2 (b) for all samples. The activation energy values were calculated and listed in Table 1.The specimens with 5wt. % of Al_2O_3 showed lower activation energy than the samples of other components, which indicated that addition of Al_2O_3 modifies the matrix and the primary crystallization becomes simple.

3.2 XRD analysis and Rietveld refinement of LMZBS+Al_2O_3 glass-ceramics

For the sake of investigating the sintering crystallization behavior of (100-x) (Li_2O-MgO-ZnO-B_2O_3-SiO_2) +xAl_2O_3, (x=1~10wt. %.) (LMZBSA) glass-ceramics,

the glass-ceramics were prepared and sintered at different temperatures 880□~940□ for 2h. The XRD patterns of LMZBSA glass-ceramics with different Al_2O_3 contents sintered at 900□ for 2h are illustrated in Fig.3 (a), and different sintering temperature with 5wt. % Al_2O_3 are shown in Fig.3 (b). As shown, the diffraction peaks are assigned to $Mg_2B_2O_5$ (PDF#86-0531), Li_2ZnSiO_4 (PDF#15-0056), $ZnAl_2O_4$ (PDF#74-1136) and $LiAlSiO_4$ (PDF#26-0839), respectively. The crystalline phase $Mg_2B_2O_5$ (PDF#86-0531) is always the main phase in Fig.3 (a). The peak intensities of $LiAlSiO_4$ and $ZnAl_2O_4$ are gradually enhance with the increase of the sintering temperature or the content of Al_2O_3. However, the content of crystal phase Li_2ZnSiO_4 decreases with the increase of Al_2O_3 content in LMZBSA glass-ceramics. Obviously, the phases of Li_2ZnSiO_4 and Al_2O_3 reacted during the sintering process to generate $LiAlSiO_4$ and $ZnAl_2O_4$. Therefore, the chemical reaction between Li_2ZnSiO_4 and Al_2O_3 could be described as:

$$Li_2ZnSiO_4+Al_2O_3 \rightarrow LiAlSiO_4+ZnAl_2O_4 \qquad (5)$$

To further illustrate the impact of the Al_2O_3 content on the LMZBSA glass-ceramics, the information of crystal structure and composition content can be obtained by refining the XRD data with EXPGUI-GSAS program. Rietveld plot for LMZBSA glass-ceramics sintered at 900℃ is shown in Fig.4 (a) to (e).The result of refined and calculated are listed in Table 2.

The compactness of the composite system was evaluated by measuring the relative density of the sintered LMZBSA glass-ceramics. The relative density of glass ceramics can be obtained by equation (6) [16-18]:

$$\rho_{relative} = \frac{\rho_{bulk}}{\rho_{theo}} \qquad (6)$$

Where ρ_{bulk} is the bulk density measured by the Archimedes principle, the theoretical density was calculated from the following equation (7) and (8)[16, 17]:

$$\rho_1 = \frac{A \times Z}{V \times N} \qquad (7)$$

$$\rho_{theo} = (W_1 + W_2 + W_3 + W_4)\left(\frac{W_1}{\rho_1} + \frac{W_2}{\rho_2} + \frac{W_3}{\rho_3} + \frac{W_4}{\rho_4}\right)^{-1} \qquad (8)$$

Where 1, 2, 3, 4, *W*, *A*, *Z*, *V*, *N* represents $Mg_2B_2O_5$(PDF 86-0531), Li_2ZnSiO_4 (PDF 15-0056), $ZnAl_2O_4$(PDF 74-1136)，$LiAlSiO_4$(PDF 26-0839), weight fraction, number of atoms in the unit cell, atomic weight, volume of unit cell and Avogadro number, respectively. The calculated values of the theoretical density are shown in Table2.

When the specimens sintered at 900℃ with different amounts of Al_2O_3 and 880 – 900℃ with 5wt. % Al_2O_3, the mass fractions of $Mg_2B_2O_5$ (PDF 86-0531) and Li_2ZnSiO_4 (PDF 15-0056) phases decreased while those of $ZnAl_2O_4$ (PDF 74-1136) and $LiAlSiO_4$ (PDF 26-0839) phases increased, which is comply with the XRD results shown in Fig.3 (a) and (b). Indeed, the mentioned results verified that the proportions of raw materials and sintering temperature had a great influence on the composition of LMZBSA glass-ceramics sample.

Fig.5 (a) to (e) displays the surface morphology of LMZBSA glass-ceramics with 1-10wt. % Al_2O_3 sintering at 920℃ for 2h. Fig.5 (f) to (h) shows the surface morphology LMZBSA glass-ceramics sintered at 880-940℃ with 5wt. % Al_2O_3. Fig.5 (c) presented three kinds of grains, including stick-like grain A, matrix grain B, small granule grain C. With increasing Al_2O_3 addition [Fig.5 (a) to (e)], the stick-like grain A and matrix grain B decreased slightly, the small granule C increase obviously. In addition, as shown in Fig 5(c) and (f) to (h), When the content of Al_2O_3 is constant, the stick-like grain A grows significantly with the increase of sintering temperature. At 920 °C, obvious pore morphology was detected for LMZBSA with 5wt. % Al_2O_3. LMZBSA glass-ceramics containing 5wt. % of Al_2O_3 appeared liquid phase when sintered at 950℃, which caused by overheating.

The bulk density of the LMZBSA glass-ceramics is shown in Fig.6 (a), the flexural strength and relative density of LMZBSA glass-ceramics with 1-10wt. % Al_2O_3 sintering at 900℃ are shown in Fig.6 (b). Form Fig.6 (a), the LMZBSA glass-ceramics reaches to a maximum density of 3.213g/cm^3 at 900℃ for 10wt. % Al_2O_3. And with the variation of in Al_2O_3 content, the bulk density continues to increase, in which is attributed to the appearance of higher density of $ZnAl_2O_4$ (ρ=4.6322 g/cm^3). Glass-ceramics sintered at 920℃ always have the lowest bulk density, which is consistent with the phenomenon observed in Fig. 5, because of the largest porosity.

The relative density of glass-ceramics sinter at 900□ with 1-10wt. % Al2O3 increases at first, and then declines. The glass-ceramics gets a maximum relative density of 96.41% at 900□ for 5wt. % Al_2O_3, which means the glass-ceramics can be sintered to the most compact at 900□ with 5wt. % Al_2O_3.

The variation of LMZBAS's flexural strength with 1~10wt. % Al_2O_3 are shown **F**ig.6 (b). At first, the flexural strength increased from 140MPa at x=1wt. % to 190MPa (This flexural strength is 20% higher than the sample made by Xie et al. [11], and the sintering temperature is lower.) at x=5wt. %, afterward, it went down to 160MPa at x = 10wt. %. The flexural strength of the LMZBSA glass-ceramics was related to its internal structure and the relative density. With the content of Al_2O_3 increases, the smaller and finer granular crystal phases gradually increase. The stick-like grain can be regarded as the main frame, meanwhile, the increasing number of small particles are filled in the gap of the support frame. Hence, the denseness of the glass ceramic is increased, and the flexural strength also increases. Obviously, when LMZBSA glass-ceramics sintered at 900□ with 5wt. % Al_2O_3, the densification of the microstructure is optimal, which is consist with the maximized flexural strength. When the glass-ceramics sintered at 900□ with more than 5wt. % Al_2O_3, the decline of flexural strength is ascribed to the decrease of relative density. Then, when the temperature continues to rise, the stick-like grains gradually grow abnormally and disappear and the flexural strength decreases. The flexural strength results are listed in Table 3.

The chemical components of A, B and C in the marked area shown Fig.5 (c) was identify by EDS (The EDS device cannot detect Li and B). The results of EDS testing for the marked areas are shown Fig.7. The results reveals that all regions contained O (fuchsia), Mg (red), Si (yellow), Al (wathet) and Zn (green). Zone A is mainly rich in Mg and O, Mg: O is 3.7:10, and the ratio is close to 1:2.5. The B area are mainly composed of O, Si and Zn. The region C are mainly O, Al, Zn. Combining the XRD patterns (Fig.4) analysis, we can speculate that the A region of the stick-like grains is $Mg_2B_2O_5$ (PDF#86-0531). B area of the matrix grain is Li_2ZnSiO_4 (PDF#15-0056), Area C of the small granule grain is a concentrated area of $LiAlSiO_4$ (PDF#26-0839)

and $ZnAl_2O_4$ (PDF#74-1136). Because $Mg_2B_2O_5$ (PDF#86-0531) phase is the most abundant in the sample, it can also be observed from Fig.5 (c). $Mg_2B_2O_5$ (PDF#86-0531) phase is always unavoidable when selecting EDS measurement area, so the measurement results in A, B and C region always show a large amount of Mg.

3 .3 Dielectric properties of LMZBAS glass-ceramics

The measured ε_r values and calculated ε_r values of the samples sintered at 900□ are shown in Fig.8. As known, the ε_r value is affected by relative density, crystal structure, and composition phase[19]. In our work, the relative density results suggested a compact samples were obtained, and there are apparently different in compositions. Hence, the variation of ε_r is ascribed to the various component and the content of each phase. The effect of multiphase glass-ceramic on the dielectric constant can be expressed by mixing rule [20, 21]:

$$\varepsilon = V_1\varepsilon_1 + V_2\varepsilon_2 + V_3\varepsilon_3 + V_4\varepsilon_4 \quad \text{(Parallel mixing model)} \quad (9)$$

$$\ln\varepsilon = V_1\ln\varepsilon_1 + V_2\ln\varepsilon_2 + V_3\ln\varepsilon_3 + V_4\ln\varepsilon_4 \quad \text{(Logarithmic mixing model)} \quad (10)$$

Where V_1, V_2, V_3, V_4 represents the volume fraction of $Mg_2B_2O_5$, Li_2ZnSiO_4, $LiAlSiO_4$ and $ZnAl_2O_4$; ε_1, ε_2, ε_3, ε_4 represents the dielectric constant of $Mg_2B_2O_5$, Li_2ZnSiO_4, $ZnAl_2O_4$ and $LiAlSiO_4$, respectively.

Since $Mg_2B_2O_5$ (ε_r=7.2, $Q\times f$=18400GHz, τ_f=-46ppm/□)[22], Li_2ZnSiO_4 (ε_r=5.8, $Q\times f$=14700GHz, τ_f=-47.2ppm/□)[23], $ZnAl_2O_5$(ε_r=8.5, $Q\times f$=56300GHz, τ_f=-79ppm/□)[24] and $LiAlSiO_4$ (ε_r=4.8, $Q\times f$=36000GHz, τ_f=8ppm/□)[25], has a similar dielectric constant in the microwave frequency range, the intrinsic property of the crystal phase does not cause a significant change in ε_r with an increase in the Al_2O_3 content. The ε_r was changed slightly from 6.6 to 6.9 as shown in Fig.9. It can be seen from the experimental test data that the dielectric constant decreases first and then augment slowly. The decrease in dielectric constant of the LMZBSA glass-ceramics is contributed to the formation of $LiAlSiO_4$ (ε_r=4.8) at the beginning of the addition of Al_2O_3. When the content of Al_2O_3 is continuously increased, $ZnAl_2O_4$ phase (ε_r=8.5) is formed in large quantities, the dielectric constant of the LMZBAS glass-ceramics are increase. It can be concluded that when the Al_2O_3 content is low,

the amount of $LiAlSiO_4$ is large, while with more Al_2O_3 content, the amount of $ZnAl_2O_4$ is increasing. This is consistent with the results of the mass percentage of each phase obtained after finishing in Table 2. Fig.9 shows that the Logarithmic mixing model exhibits the best predictability.

Fig.9 shows the measured $Q\times f$ value and the calculated $Q\times f$ value. The $Q\times f$ value is determined by the internal and external losses[26]. The intrinsic loss is derived from the lattice anharmonic, while extrinsic loss includes the second phase, defect and so on. Since there are four phases in this sample，it is hard to acquire the lattice parameters through the combination of the overall modes. Therefore, we mainly discuss the impact of external loss. Such as relative density and the content of each phase in the LMZBAS glass-ceramics.

Combining the previous discussion, with **F**ig.8, when the Al_2O_3 content is 1-5wt. %, the relative density of the LMZBAS glass ceramic is gradually increased, and the $Q\times f$ value increased as well. In addition, $Q\times f$ is consistent with the famous empirical model for multiphase glass-ceramics, as described follows[21, 22]:

$$(Q\times f)^{-1} = V_1(Q\times f)_1^{-1} + V_2(Q\times f)_2^{-1} + V_3(Q\times f)_3^{-1} + V_4(Q\times f)_4^{-1} \qquad (11)$$

Where $V_1.V_2,V_3,V_4$ represents the volume fraction of $Mg_2B_2O_5$, Li_2ZnSiO_4, $ZnAl_2O_4$ and $LiAlSiO_4$; $(Q\times f)_1$,$(Q\times f)_2$,$(Q\times f)_3$,$(Q\times f)_4$ represents $Q\times f$ value of $Mg_2B_2O_5$, Li_2ZnSiO_4, $ZnAl_2O_4$ and $LiAlSiO_4$,respectively. With the increase of Al2O3 content in LMZBAS glass-ceramics, the calculate $Q\times f$ value keep going up, which is due to the variation content of $ZnAl_2O_4$ phase with a high $Q\times f$ value. However, the actual measured $Q\times f$ value is increased first (Al_2O_3 content is 1-5wt. %) and then decreased (Al_2O_3 content is 5-10wt. %). Because there are many phases in the sample, and the $ZnAl_2O_4$ and $LiAlSiO_4$ crystal phase are small particles, excessive $ZnAl_2O_4$ and $LiAlSiO_4$ crystal phase will lead to an increase in the number of grain boundaries, which will have a negative influence on the $Q\times f$ value. Moreover, when the content of Al_2O_3 is high, the decrease in relative density is also the cause of the decrease in $Q\times f$ value. The glass-ceramics gets a maximum $Q\times f$ value (12500GHz, at 12.8GHz) at 900℃ for 5wt. % Al_2O_3.

The variation of measured τ_f values and calculated τ_f values are showed in **F**ig.9. From previous reports, the calculated τ_f value can be obtained from the following [20-22]:

$$\tau_f = V_1\tau_{f1} + V_2\tau_{f2} + V_3\tau_{f3} + V_4\tau_{f4} \quad (12)$$

Where V_1.V_2, V_3, V_4 represents the volume fraction of $Mg_2B_2O_5$, Li_2ZnSiO_4, $LiAlSiO_4$ and $ZnAl_2O_4$; τ_{f1}, τ_{f2}, τ_{f3}, τ_{f4} represents value of $Mg_2B_2O_5$, Li_2ZnSiO_4, $LiAlSiO_4$ and $ZnAl_2O_4$, respectively. The calculated value starts to increase, which is attributed to the positive value of $LiAlSiO_4$ (8ppm/□). Later, the calculated value growth was slowly because the $ZnAl_2O_5$ (-79ppm/□) phase had a negative impact. The actual τ_f values are between -53ppm/□ and -43ppm/□, and the calculated τ_f values are between -46ppm/□and -44ppm/□.Combining with the measured and calculated τ_f values, it can be found that the effect of Al_2O_3 on τ_f value is not obvious. The dielectric properties of glass ceramic samples of other components are listed in Table3.

4. CONCLUSION

In the present work, LMZBSA glass-ceramics were prepared by conventional solid-phase sintering. According to Dietzel, Saad-Paulin methods and Kissinger model, the presence of Al_2O_3 in the glass composition significantly improves the GFA and reduced activation energy, which is beneficial for the initial crystallization of LMZBSA glass-ceramics. LMZBSA glass-ceramics containing 5wt. % Al_2O_3 sintered at 900□ can obtain a maximum relative density (96.41%) and maximum flexural strength (190MPa) and optimal microwave dielectric properties (ε_r=6.8, $Q\times f$=12500GHz, τ_f=-45ppm/□). The glass-ceramics can be sintered at a lower temperature and is suitable for a fully dense and high-strength dielectric substrate with a low dielectric constant.

5. REFERENCES

[1] Y. Imanaka, Multilayers low temperature cofired ceramics (LTCC) technology, Springer, (2005)

[2] B. Geller, B. Thaler, A. Fathy, M.J. Libertatore, H.D. Chen, G. Ayers, V. Pendrick, Y. Narayan, LTCC-M: an enabling technology for high performance multilayer RF systems, Microw. J. (1999) 42

(7) 64–72.

[3] M.T. Sebastian, H. Jantunen, Low loss dielectric materials for LTCC applications: a review, Int. Mater. Rev. 53 (2) (2008) 57–90.

[4] Zhou J, Towards rational design of low-temperature co-fired ceramic (LTCC) materials. J Adv Ceram. (1) (2012) 89-99.

[5] Naoya Mori, Yasutaka Sugimoto, Jun Harada,Yukio Higuchi, Dielectric properties of new glass-ceramics for LTCC applied to microwave or millimeter-wave frequencies, Journal of the European Ceramic Society. (26) (2006) 1925–1928

[6] Xiangyu Du, Hua Su, Huaiwu Zhang, Zhenhua Zhou,Yulan Jing, Gongwen Gan. High-Q microwave dielectric properties of $Li(Zn_{0.95}Co_{0.05})_{1.5}SiO_4$ ceramics for LTCC applications, Ceramics International. (43) (2017) 7636–7640.

[7] K.M. Manu, P.S. Anjana, M.T. Sebastian, Low permittivity $SrCuSi_4O_{10}$–LMZBS glass composite for LTCC applications, Materials Letters. (65) (2011) 565–567.

[8] Sumesh George, Prabhakaran Sreekumari Anjana, Vasudevan Nair Deepu, Pezholil Mohanan, Mailadil Thomas SEbastian, Low-Temperature Sintering and Microwave Dielectric Properties of Li_2MgSiO_4 Ceramics, J. Am. Ceram. Soc. 92 (6) (2009) 1244–1249.

[9] Dong-Xiang Zhou,Fei Sun, Yun-Xiang Hu, Qiu Yun Fu, Gang Dou, Low-temperature sintering and microwave dielectric properties of $Mg_3B_2O_6$-LMZBS composites, J Mater Sci: Mater Electron. (23) (2012) 981–989.

[10] Gang Wang, HuaiWu Zhang, Cheng Liu, Hua Su, LiJun Jia, Jie Li, Xin Huang, GongWen Gan, Low-Temperature Sintering $Li_3Mg_{1.8}Ca_{0.2}NbO_6$ Microwave Dielectric Ceramics with LMZBS Glass, Journal of ELECTRONIC MATERIALS.Vol. 47 (8) (2018).

[11] Linshan Xie, Chaowei Zhong, Zixuan Fang,Yu Zhao, Bin Tang, Shuren Zhang. Microwave dielectric properties of Li_2O-xMgO-ZnO-B_2O_3-SiO_2 glass-ceramics (x = 30-50 wt. %), Journal of the Ceramic Society of Japan. 126 (3) (2018) 163-169.

[12] Sara Banijamali, Touradj Ebadzadeh. Glass-forming ability, sinter-crystallization behavior and microwave dielectric properties of MgO-B_2O_3-(Al_2O_3)-SiO_2 glass-ceramics, Journal of Non-Crystalline Solids. (441) (2016) 34–41.

[13] Yu Zhang, Jian Yao, Xiangyu Zhao, Liqun Ma. Ti substituted Ni-free $Zr_{65-x}Ti_xCu_{17.5}Fe_{10}Al_{7.5}$ bulk metallic glasses with significantly enhanced glass-forming ability and mechanical properties. Journal of Alloys and Compounds.(2018) 713-718

[14] F.A. Santos, J.R.J. Delben, A.A.S.T. Delben, L.H.C Andrade, S.M. Lima, Thermal stability and crystallization behavior of TiO_2 doped ZBLAN glasses, Journal of Non-Crystalline Solids. (357) (2011) 2907–2910.

[15] Cosmas M. Muiva, Stephen T. Sathiaraj, Julius M. Mwabora, Crystallisation kinetics, glass forming ability and thermal stability in glassy Se100 - xInx chalcogenide alloys, Journal of Non-Crystalline Solids. (357) (2011) 3726–3733

[16] Yonggui Zhao, Ping Zhang, Complex chemical bond theory, Raman spectra and microwave dielectric properties of low loss ceramics $NdNbO_4$–xAl_2O_3, J Mater Sci: Mater Electron. (27) (2016) 2511–2522

[17] Hongyu Yang, Enzhu Li, Hongchen Yang, Hongcai He, Ren S. Zhang, Synthesis of $Zn_{0.5}Ti_{0.5}NbO_4$ microwave dielectric ceramics with Li_2O-B_2O_3-SiO_2 glass for LTCC application, Int J Appl Glass Sci. (00) (2017) 1-11.

[18] Enzhu Li, Hongcheng Yang, Hongyu Yang, Shuren Zhang, Effects of Li2O-B2O3-SiO2 glass on

the low-temperature sintering of Zn0.15Nb0.3Ti0.55O2 ceramics, Ceramics International. (44) (2018) 8072-8080

[19] Enzhu Li, Na Niu, Jing Wang, Shaoyang Yu, Shuxin Duan, Ying yuan, Effect of Li-B-Si glass on the low temperature sintering behaviors and microwave dielectric properties of the Li-modified ss-phase Li2O-Nb2O5-TiO2 ceramics, J Mater Sci: Mater Electron. (26) (2015) 3330-3335

[20] Jian Zhang, Ruzhong Zuo, Jie Song, Yudong Xu, Min Shi, Low-loss and low-temperature firable $Li_2Mg_3SnO_6$-$Ba_3(VO_4)_2$ microwave dielectric ceramics for LTCC applications, Ceramics International. (44) (2018) 2606–2610.

[21] Weiqiong Liu, Ruzhong Zuo, A novel Li_2TiO_3–Li_2CeO_3 ceramic composite with excellent microwave dielectric properties for low-temperature cofired ceramic applications, Journal of the European Ceramic Society (38) (2018) 119–123.

[22] Urban Dosler, Marjeta Macek Krzmanc, Danilo Suvorov. The synthesis and microwave dielectric properties of $Mg_3B_2O_6$ and $Mg_2B_2O_5$ ceramics, Journal of the European Ceramic Society. (30) (2010) 413–418.

[23] Gang Dou, Dongxiang Zhou, Shuping Gong, Mei Guo. Low temperature sintering and microwave dielectric properties of Li_2ZnSiO_4 ceramics with ZB glass, J Mater Sci: Mater Electron. (24) (2013) 1601–1607.

[24] Sang-Hyo Kweon, Mi-Ri Joung, Jin-Seong Kim,BoYun Kim, Sahn Nahm, Jong-Hoo Paik, Young Sik Kim, Tae Hyun Sung, Low Temperature Sintering and Microwave Dielectric Properties of B_2O_3-added $LiAlSiO_4$ Ceramics, J. Am. Ceram. Soc. 94 (7) (2011) 1995–1998.

[25] K.P. Surendran, M.T. Sebastian, M.V. Manjusha,Jacob Philip, A low loss dielectric substrate in $ZnAl_2O_4$–TiO_2 system for microelectronic applications, JOURNAL OF APPLIED PHYSICS. (98)

(2005) 044101.

[26] Hongyu Yang, Shuren Zhang, Hongcheng Yang, Xing Zhang, Enzhu Li, Structural Evolution and Microwave Dielectric Properties of xZn0.5Ti0.5NbO4 - (1-x) Zn0.15Nb0.3Ti0.55O2 Ceramics, Inorg. Chem. (57) (2018) 8264-8275

Table 1. Characteristic temperature of the DSC curve with heating rate of 10K/min and the glass-forming ability measurements.

LMZBS+$x$$Al_2O_3$ (wt. %)	Tg (±1□)	Tx (±1□)	Tp (±1□)	ΔT(Tp - Tg) (±1□)	S (±1□)	Ea (KJ/mol)
0	776	882	915	139	4.51	265.9±31.9
1	776	886	932	156	6.51	220.8±9.8
3	776	894	937	161	6.54	218.9±10.1
5	776	900	947	171	7.51	182.1±19.4
7	777	902	955	178	8.53	262.7±32.4
10	778	907	966	188	9.95	205.0±41.3

Table 2. The result of refined and calculated of LMZBSA glass-ceramics sintered at different conditions

	Different content of Al_2O_3,*ST*=900□					5wt.% Al_2O_3,different *ST*		
	1wt.%	3wt.%	5wt.%	7wt.%	10wt.%	880□	920□	940□
W_{f1} (%)	70.45	67.90	64.17	57.81	52.59	66.30	63.57	62.88
W_{f2} (%)	26.82	25.87	21.63	19.70	17.47	24.01	21.53	21.85
W_{f3} (%)	0.84	2.66	8.55	16.91	22.77	5.07	8.74	9.08
W_{f4} (%)	1.79	3.58	5.66	7.07	8.60	4.62	6.15	6.19
ρ_1(g/cm^3)	2.9150	2.9159	2.9151	2.9137	2.9139	2.9157	2.9146	2.9153
ρ_2(g/cm^3)	3.4039	3.3948	3.4022	3.4359	3.4217	3.4136	3.4027	3.4235
ρ_3(g/cm^3)	4.6319	4.6264	4.6263	4.6322	4.6376	4.6221	4.6246	4.6258
ρ_4(g/cm^3)	2.3731	2.3863	2.3815	2.3813	2.3702	2.3875	2.3912	2.3713
ρ_{theo}(g/cm^3)	3.0293	3.0331	3.0684	3.2016	3.2130	3.0469	3.0675	3.0750
$\rho_{relative}$(%)	93.86	95.03	96.41	95.73	94.70	95.72	94.27	95.21
R_p (%)	4.41	4.52	4.68	5.51	5.25	4.51	4.79	5.21
R_{wp} (%)	5.83	5.94	6.15	7.59	7.42	5.85	6.37	7.36
χ^2	1.423	1.437	1.575	2.014	2.204	1.379	1.626	2.154

ST: sintering temperature; W_f: the mass fraction of the phase; ρ_1, ρ_2, ρ_3, ρ_4: the theoretical density of $Mg_2B_2O_5$ (PDF 86-0531), Li_2ZnSiO_4 (PDF 15-0056), $ZnAl_2O_4$

(PDF 74-1136) phase and $LiAlSiO_4$ (PDF 26-0839); R_p: reliability factor of weighted pattern; R_{wp}: reliability factor of weighted pattern; χ^2: goodness of fit.

Table 3. Variations of flexural strength (σ) and microwave dielectric properties in LMZBS+$x$$Al_2O_3$ (x=1~10wt. %) glass-ceramics

x (wt. %)	ST (□)	ε_r	$Q\times f$ (GHz)	σ(MPa)	τ_f (ppm/□)	f (Hz)
1wt.%	880□	6.77	9326	123	-52.4	12.67
3wt.%	880□	6.67	10443	139	-49.0	12.86
5wt.%	880□	6.79	10996	141	-51.7	13.01
7wt.%	880□	6.81	9821	136	-55.6	12.90
10wt.%	880□	6.84	9711	137	-56.0	12.64
1wt.%	920□	6.52	9899	113	-48.0	13.24
3wt.%	920□	6.53	10841	134	-49.6	12.87
5wt.%	920□	6.72	11235	154	-52.0	12.91
7wt.%	920□	6.48	11145	129	-52.5	13.08
10wt.%	920□	6.79	10723	137	-59.0	12.60
1wt.%	940□	6.42	7767	80	-47.3	12.90
3wt.%	940□	6.43	7283	85	-43.0	13.06
5wt.%	940□	6.50	8320	96	-49.5	13.06
7wt.%	940□	6.57	8964	102	-55.0	13.10
10wt.%	940□	6.65	8850	119	-61.0	12.78

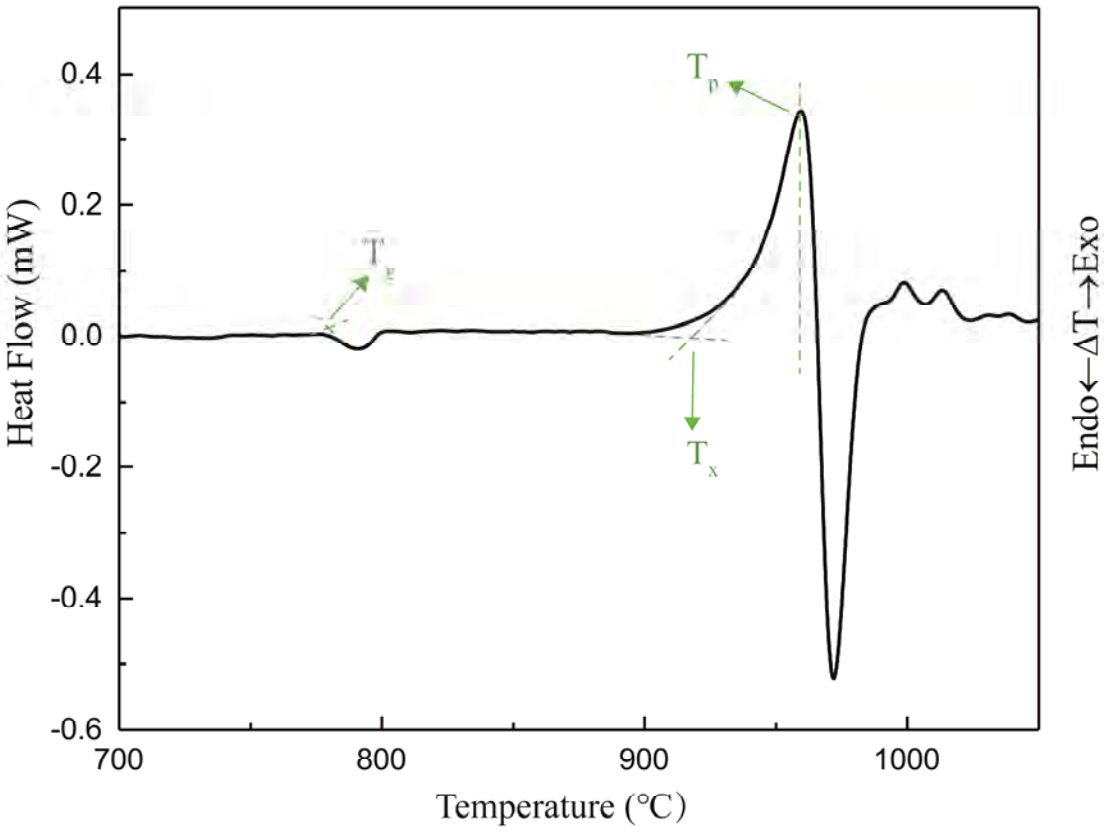

Fig.1. DSC curve for 10wt. % of Al_2O_3 doped LMZBS glass with heating rate of 10K/min.

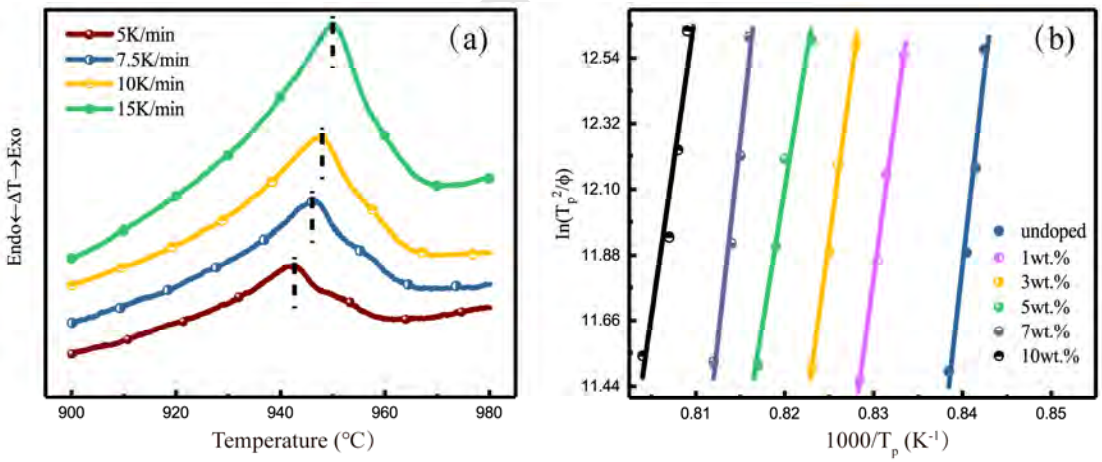

Fig.2. (a) The crystallization peak position for different heating rates for the 5wt. % of Al_2O_3-LMZBS glass; (b) The Kissinger plots for all specimens

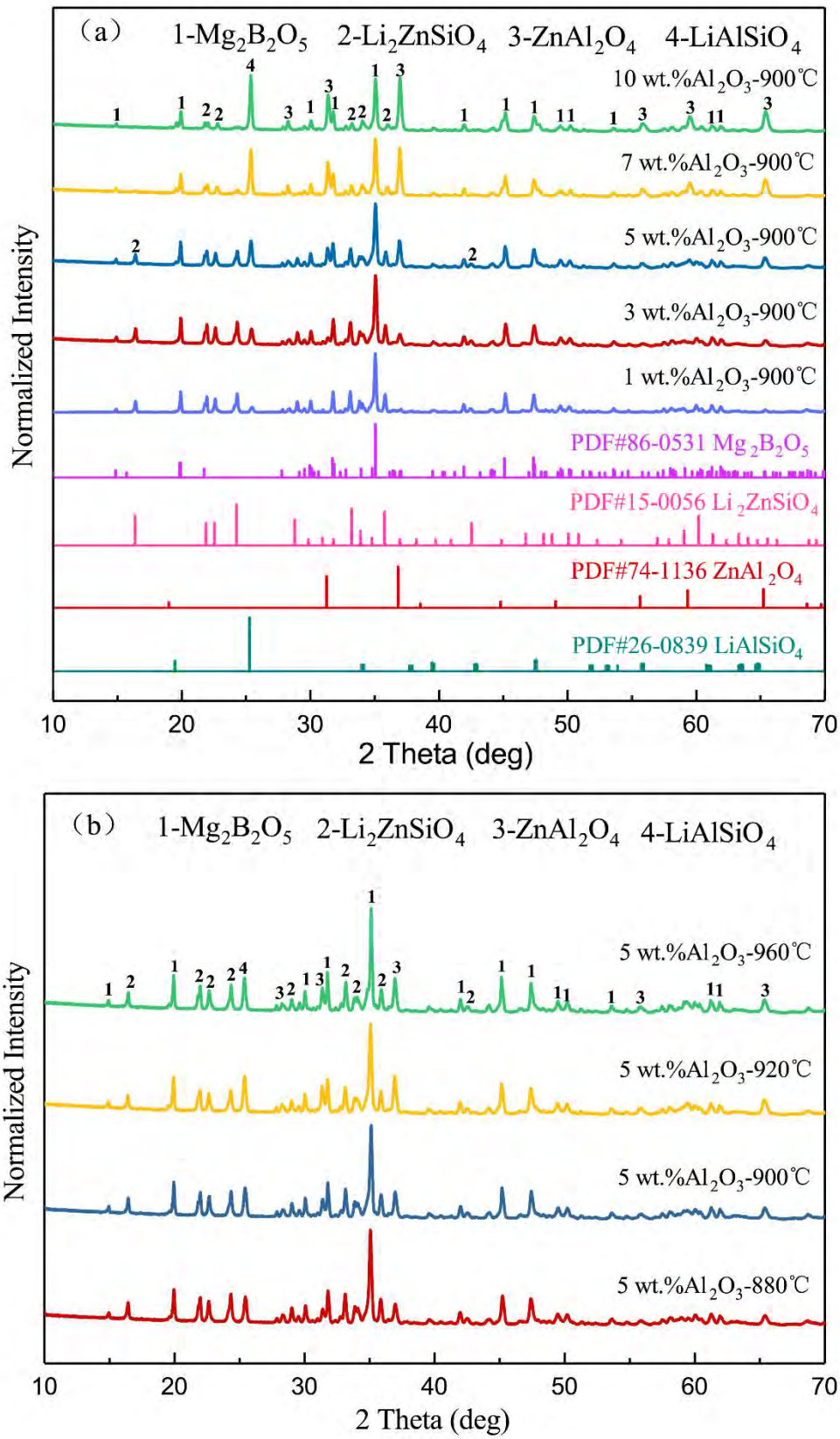

Fig.3 (a) The XRD patterns of LMZBSA glass-ceramics with different amount of Al_2O_3 sintered at 900□ for 2h in air; (b) The XRD patterns of LMZBSA glass-ceramics sintered at 880~940□ with 5wt.% Al_2O_3

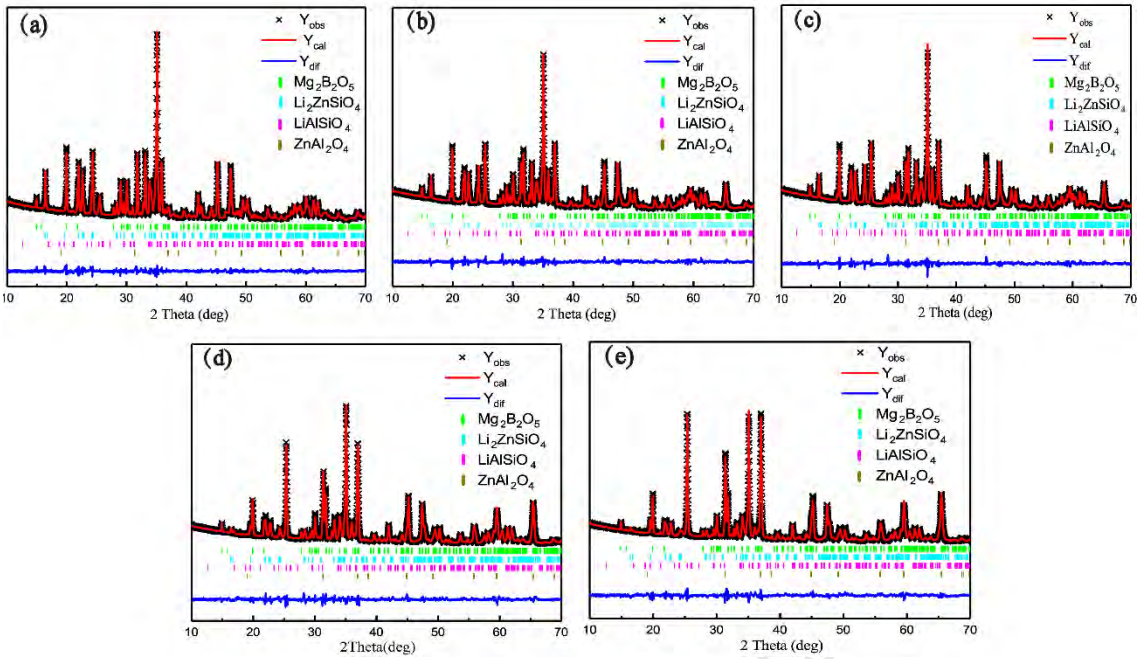

Fig.4 The refined XRD patterns of the LMZBSA glass-ceramics sintered at 900□ for 2h;(a)x=1wt.%,(b)x=3 wt.%,(c)x=5 wt.%,(d)x=7 wt.%,(e)x=10 wt.%

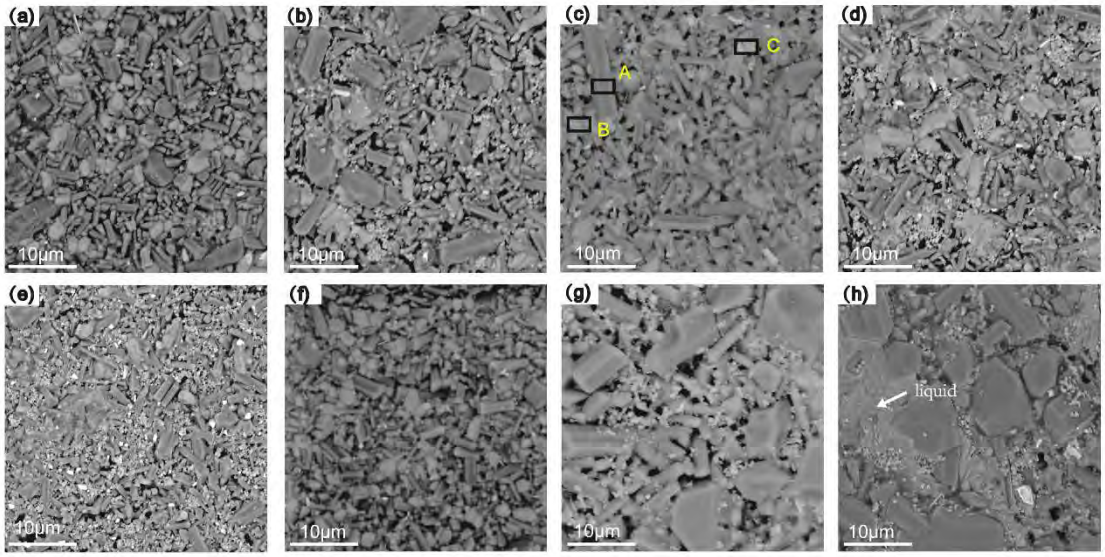

Fig.5 Surface of the LMZBSA glass-ceramics: (a)900□, with 1wt.% Al_2O_3,(b) 900□, with 3wt.% Al_2O_3,(c) 900□, with 5wt.% Al_2O_3, (d) 900□, with 7wt.% Al_2O_3,(e) 900□,

with 10wt.% Al_2O_3, (f) 880□, with 5wt.% Al_2O_3,(g) 920□, with 5wt.% Al_2O_3,(h) 940□, with 5wt.% Al_2O_3

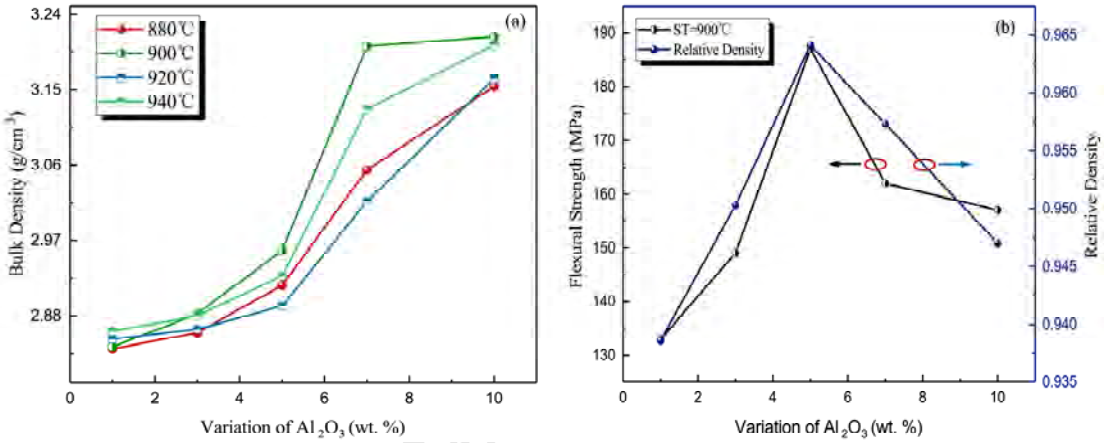

Fig.6 The bulk density, flexural strength and relative density values of LMZBAS glass-ceramics with different content of Al_2O_3 sintered at 880-940□

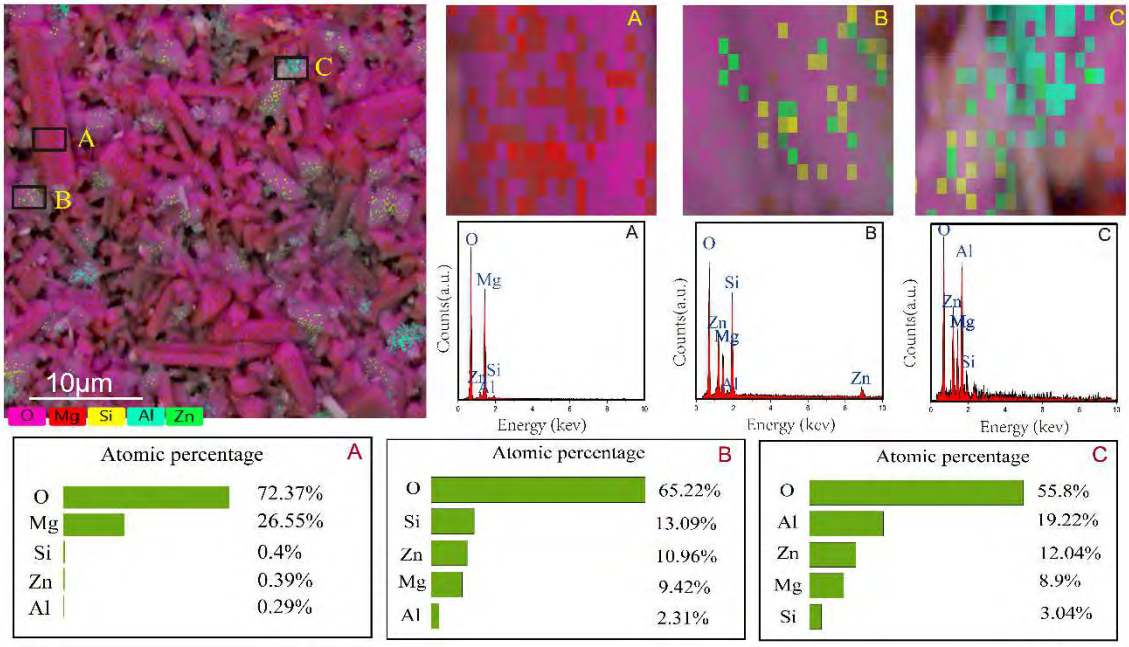

Fig.7 Energy dispersion X-ray analysis (EDS) data for LMZBSA glass-ceramic

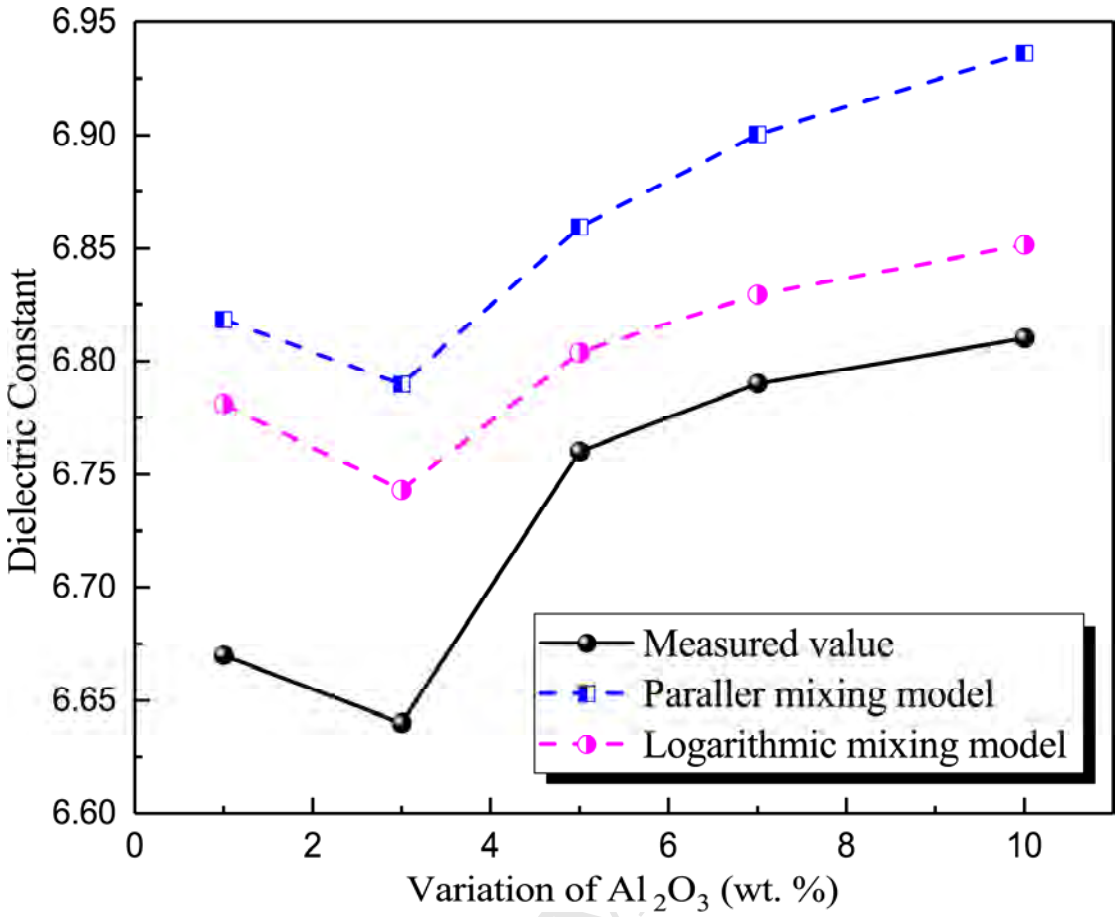

Fig.8 The calculated and measured ε_r values of LMZBAS glass-ceramic with 1~10wt. % Al_2O_3 sintered at 900□

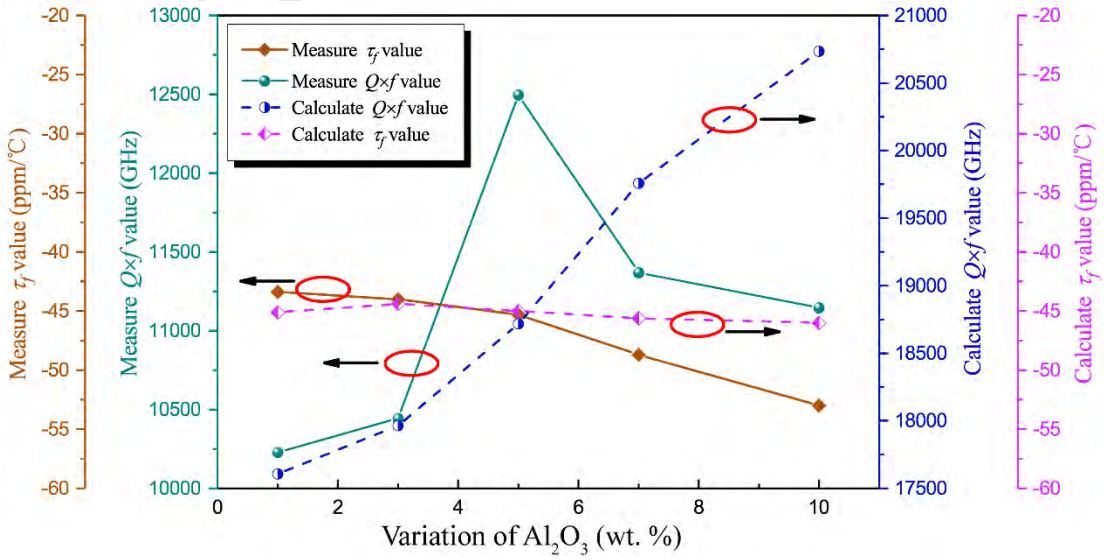

Fig.9 Changes in measured τ_f values, the measured $Q \times f$ value, the calculate $Q \times f$ value and calculated τ_f values of LMZBAS glass-ceramic with 1~10wt. % Al_2O_3 sintered at 900□